

## Article

# Investigation of Chinese-Style Greenhouse Usage Across Europe

Serkan Erdem <sup>\*,†</sup>  and Cenk Onan <sup>†</sup> 

Department of Mechanical Engineering, Yildiz Technical University, Besiktas, Istanbul 34349, Turkey; conan@yildiz.edu.tr

\* Correspondence: serdem@yildiz.edu.tr

† These authors contributed equally to this work.

**Abstract:** Chinese-style greenhouses (CSGs), characterized by a distinct geometric shape compared to traditional greenhouses, are extensively utilized in China. In this study, this type of greenhouse was modeled using TRNSYS software version 18 and experimentally validated. The model can transiently determine the indoor conditions of the greenhouse and the requirement for additional heating. It calculates the heat loss due to plant evapotranspiration as well as all the heat gains and losses from the surfaces. The application of this greenhouse has been investigated from the southernmost to the northernmost regions of Europe. For this purpose, cities located at different latitudes (between 32.63° N and 69.65° N) were entered into the model, and the results were obtained and compared. The analysis conducted over the entire year demonstrated that the CSG indoor temperature is more dependent on solar energy during the day and on outdoor temperature at night. The two southernmost cities in our survey, Funchal, Portugal (32.63° N) and Luqa, Malta (35.83° N), had no winter heating requirement. The thermal covering was sufficient to minimize night heat loss and maintain a suitable indoor temperature. In northern cities, the heating requirement was relatively high due to the lower outdoor temperature and solar radiation. Consequently, the duration of the heating season increases towards the north. In the northernmost city, Tromso, Norway (69.65° N), the heating season was determined to last 12 months. In the absence of solar energy, the transparent surface of the greenhouse is covered with thermal insulation to prevent heat loss. It has been shown that with the appropriate selection of this thermal covering, which is controlled based on the presence of instantaneous solar energy, up to 80% savings can be achieved from additional heating in southern cities. In the north, this rate can be increased up to a maximum of 70% by increasing the thermal covering thickness.



**Citation:** Erdem, S.; Onan, C. Investigation of Chinese-Style Greenhouse Usage Across Europe. *Energies* **2024**, *17*, 5435. <https://doi.org/10.3390/en17215435>

Academic Editor: Xi Chen

Received: 7 October 2024

Revised: 26 October 2024

Accepted: 28 October 2024

Published: 31 October 2024



**Copyright:** © 2024 by the authors. Licensee MDPI, Basel, Switzerland. This article is an open access article distributed under the terms and conditions of the Creative Commons Attribution (CC BY) license (<https://creativecommons.org/licenses/by/4.0/>).

**Keywords:** transient analysis; heating; solar greenhouse; energy consumption

## 1. Introduction

Chinese-style solar greenhouses (CSGs) are structures characterized by a curved, transparent south-facing roof and a massive north wall (Figure 1). These greenhouses are named as such because they are utilized for vegetable cultivation in the northern regions of China. In the 1930s, a basic CSG was established in southern Liaoning Province, China, primarily for the winter cultivation of leafy vegetables. Over time, advancements in materials and construction techniques have enabled the cultivation of not only vegetables but also fruits in these greenhouses, without the need for additional heating. This was achieved despite significant temperature differences of 21 °C to 25 °C between the interior and exterior, particularly in regions between 32° N and 41° N in China [1]. Depending on external conditions and design, CSGs can function as completely passive systems or with additional heating. The indoor air conditions of a CSG are crucial due to the plants grown. To accurately determine these air conditions, some studies have attempted to model the indoor conditions of CSGs using mathematical models. Chen and Liu [2] mathematically modeled a lean-to greenhouse with a north wall and compared it with experimental data, revealing results for a more efficient greenhouse design. Meng et al. [3] developed a detailed

model that considers the effect of all components of the greenhouse on heat transfer to predict the internal temperatures of the CSG. The equations of the model are solved using MATLAB, and an interface is created using VB. Singh et al. [4] developed a mathematical model for predicting the internal temperatures of a greenhouse and implemented this model in C++. In their experimental validation, they stated that the simulation results were in agreement with the experimental results. Ma et al. [5] developed a dynamic model (RGWSRHJ) that can determine the indoor temperature depending on the outdoor conditions for CSGs using finite difference numerical methods. This model calculates on a completely passive system without additional heating. CFD analysis is widely used to determine the indoor conditions of CSGs. Tong et al. [6] created a time-dependent CFD model that simulates the indoor temperature based on variable outdoor weather conditions. They validated the simulation results with three days of experimental data from northern China. Wang et al. [7] incorporated a radiation model into the CFD model to predict the CSG indoor conditions, stating that this allowed for better determination of convective and radiative heat transfers. Zhang et al. [8] developed a 3D CFD model and demonstrated the relationship between the ventilation openings of the greenhouse and indoor humidity, confirming their results with a scaled experimental model. They revealed the relationship between the energy balance model and the CFD model, stating that increased ventilation openings enhanced natural ventilation, thereby reducing indoor temperature and humidity. Vivekanandan et al. [9] examined six different greenhouse geometries used for drying, concluding that the Quonset shape was the most suitable, as verified by their CFD model and experimental validation.



**Figure 1.** Typical Chinese-style solar greenhouse [1].

In a CSG, it is crucial that the indoor temperature does not fall below a minimum threshold during winter to ensure optimal plant growth. Therefore, an additional heater should be employed if necessary. Beshada et al. [10] conducted an experimental study on the efficiency of CSGs under winter conditions in Canada. They documented the temperature variations within the greenhouse and the necessity for supplementary heating. Their findings indicated that the indoor temperature of the greenhouse is more influenced by solar radiation than by the outdoor temperature. Ahamed et al. [11] developed a MATLAB-based model (CSGHEAT) to calculate the hourly heating requirements for a CSG, which they validated with experimental data. They subsequently compared this model with the TRNSYS model, which also performs transient system analysis [12]. They noted that the TRNSYS model requires further development, particularly in terms of thermal cover and moisture gain, to accurately predict the greenhouse micro-climate. Dong et al. [13] enhanced Ma et al.'s [5] model and developed the SOGREEN model, capable of calculating the necessary heating to maintain specific indoor climate conditions. This model was validated with experimental data from a greenhouse in Canada. Their results showed that the heating demand of the greenhouse is primarily dependent on the availability of solar radiation. They reported that the annual heating requirement of the CSG is 55% lower than that of a conventional greenhouse. Liu et al. [14] developed a one-dimensional transient

model to determine the internal temperature and humidity of the CSG. They stated that their user-friendly model, based on energy balance, could predict the greenhouse indoor conditions using weather forecasts.

Currently, the prevalence of poorly designed structures, substandard materials, and insufficient supervision has underscored the critical need for high-quality CSG building standards [1]. Various studies have been conducted on the geometries of CSGs to address this gap. The geometric configurations of these structures significantly influence their solar energy absorption capacity. Wei et al. [15] conducted an experimental investigation on the back wall structure of greenhouses in China, comparing three types: a fully-removable back wall CSG (FRG), a half-removable back wall CSG (HRG), and a single-span greenhouse (SPG). During the summer, the back wall was removed for ventilation purposes. Their findings indicated that the FRG maintained the lowest temperature in summer, while the SPG exhibited the highest temperature. Mobtaker et al. [16] developed a dynamic model to predict indoor temperatures for six different greenhouse geometries in northwest Iran. They reported that a single-span greenhouse oriented east-west received approximately 8% more solar radiation compared to other configurations. Chen et al. [17] examined solar radiation capture at various latitudes ( $20^{\circ}\text{K}$ – $30.6^{\circ}\text{K}$ ) for different greenhouse geometries commonly used in China. They constructed a mathematical model and implemented it in MATLAB, revealing that the sawtooth shape achieved the highest solar capture rate across all latitudes. Zhang et al. [18] explored the impact of altering the front shape of CSGs on solar capture rates. They observed that a flatter front cover enhanced solar energy capture by the soil and back wall. They concluded that the two optimal front cover geometries they identified increased night temperatures by  $2^{\circ}\text{C}$  compared to conventional designs. Liu et al. [19] aimed to enhance thermal insulation and heat storage by modifying the back wall of the CSG. They established an experimental system in China and tested it during winter, demonstrating that the new system would improve performance, particularly in high latitudes and cold regions. The indoor temperature of a greenhouse is influenced by the thermal resistance and specific heat of the north wall. Various studies have been conducted to optimize this structural element and, consequently, the greenhouse's performance. Wang et al. [20] simulated and analyzed CSGs with three different north wall structures in Northern Jiangsu Province, China. They discovered that the back wall could be thermally divided into three layers, enhancing system performance through such designs. Yu et al. [21] developed a numerical model using CFD, based on experimental data, to optimize the greenhouse back wall structure. This model enabled them to determine the temperature distribution within the greenhouse. They asserted that the optimization results for different wall heights and thicknesses would facilitate the construction of energy-efficient greenhouses. Given that the indoor conditions of a greenhouse are closely tied to the solar energy it receives, the greenhouse's positioning is also crucial. Sethi [22] modeled five different greenhouse geometries and assessed the total radiation entering the greenhouse at various latitudes, concluding that an east-west orientation is optimal at all latitudes. Gupta et al. [23] analyzed a greenhouse in New Delhi, India, using 3D-shadow analysis in Auto-CAD, and found that orientation had minimal effect on the total solar fraction. However, they noted that rotating a greenhouse initially oriented east-west by  $45^{\circ}$  clockwise resulted in the lowest radiation loss in winter and maximum loss in summer. El-Maghlany et al. [24] investigated greenhouse orientation across different locations in Egypt, concluding that south-facing greenhouses captured the most heat. Çakır and Şahin [25] examined five different greenhouse geometries initially oriented south, rotating them  $1^{\circ}$  in the east-west direction between  $0^{\circ}$  and  $90^{\circ}$ . They determined that the elliptical greenhouse shape was the optimal design for Bayburt, Turkey. Stanciu et al. [26] compared a vegetable greenhouse in Romania in terms of north-south and east-west orientation, finding that both summer cooling loads and winter heating loads were lower in the east-west orientation. Chen et al. [27] studied the orientation of CSGs at different latitudes ( $32^{\circ}\text{N}$ – $46^{\circ}\text{N}$ ) in China, using Extreme Value Theory to propose a model that determines the optimal orientation based on latitude.

Numerous studies have been carried out in the literature about CSGs, which are widely used in greenhouse cultivation. These include modeling greenhouse indoor conditions, determining additional heater/cooler requirements, and examining the effects of greenhouse geometry or structural elements. Some studies have investigated the effects of several types of greenhouses in limited areas, depending on latitude. However, no study has been conducted on the performance of CSGs across Europe. This study aims to fill that gap. In this study, a CSG model was created using the Transient System Analysis (TRNSYS) software, which is widely used for energy analysis of solar energy systems, and then the model was validated with experimental data from the literature. Subsequently, the performance of the designed CSG in different geographical locations was examined. For this purpose, geographical points were selected to simulate CSG performance, from the southernmost point of Europe to the northernmost point. CSG indoor temperatures and heating requirements are presented in comparison with each other. Additionally, the effects of using thermal coverings of different thicknesses on the total heating requirement were also revealed. Thus, the paper can demonstrate the thermal performance of using CSGs in different geographical regions and latitudes.

## 2. Materials and Method

### 2.1. CSG Model

A CSG, whose side view is shown in Figure 2, is positioned in the northern hemisphere with the wall side facing north. Thus, it ensures that more solar energy is captured from the south-facing transparent part. The north wall helps reduce the need for additional heating at night by storing the heat absorbed from the sun during the day. A thermal covering is deployed on the transparent surface at night. It is a structure that can be deployed when needed and retracted afterward. It blocks the passage of solar energy and heat transfer. With these properties, it is deployed at night to prevent the greenhouse from losing heat when there is no solar energy and retracted when the sun rises, and the outside temperature begins to increase. This significantly contributes to energy savings by reducing the need for additional heating at night. Additionally, if the temperature inside the greenhouse becomes too high, the thermal covering can be deployed to prevent overheating.

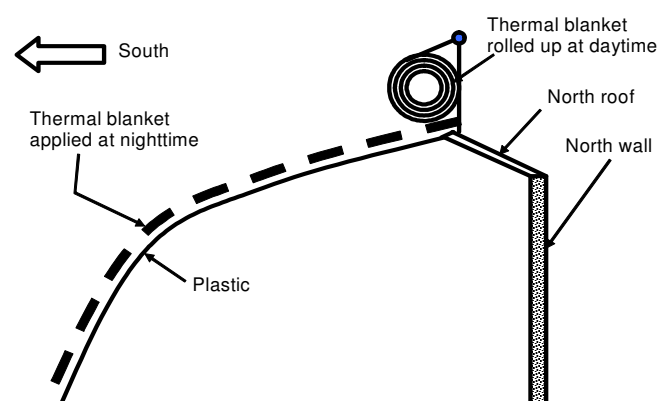


Figure 2. Side view of a CSG [10].

In addition to conduction, convection, and radiation heat gains and losses from surfaces, significant heat loss in greenhouses is caused by vegetables, fruits, or plants grown in the greenhouse. As they grow, they increase the heat load through transpiration and evaporation [28]. This situation also produces moisture, causing an increase in indoor humidity. This heat transfer mechanism, called evapotranspiration ( $Q_e$ ), can be determined as follows [29] with moisture transfer rate ( $M_T$ ) and latent heat of water vaporization ( $L_v$ ):

$$Q_e = M_T L_v \quad (1)$$

$$M_T = A_p \rho_{air} \frac{(w_{ps} - w_i)}{(R_a + R_s)} \quad (2)$$

$A_p$  is the area of the plant and  $\rho_{air}$  is the density of air. The saturated humidity ratio at the plant temperature ( $w_{ps}$ ) and the humidity ratio at the indoor air temperature ( $w_i$ ) are calculated with [30]:

$$w_{ps} = 0.6219 \times \frac{P_{ws}}{(P - P_{ws})} \quad (3)$$

$$w_i = 0.6219 \times \frac{P_w}{(P - P_w)} \quad (4)$$

Here,  $P$ ,  $P_w$ , and  $P_{ws}$  are atmospheric pressure, partial pressure of the water vapor, and partial pressure at saturation, respectively. The aerodynamic resistance and the stomatal resistance are calculated with [31,32] using characteristic length of plant leaves ( $L_f$ ), indoor airspeed ( $v_i$ ), transmissivity of cover ( $\tau$ ), and global solar radiation on the horizontal surface ( $I_g$ ):

$$R_a = 220 \times \frac{L_f^{0.2}}{v_i^{0.8}} \quad (5)$$

$$R_s = 200 \times \left( 1 + \frac{1}{\exp[0.05 \times (\tau I_g - 50)]} \right) \quad (6)$$

## 2.2. TRNSYS Model

To validate the created model with experimental data, the study of Ahamed et al. [11] was used. They presented the results of their experiments as graphics, specifying the geometric dimensions, all building materials, and characteristic features of the greenhouse they worked in. Additionally, measurements taken during the experiment, such as indoor-outdoor temperature, solar radiation, cloud cover, and additional heater usage, were provided in graphical form. In the first stage, all these graphics were converted into numerical data using WebPlotDigitizer v4.4, a web-based plot digitizer software (Figure 3). Consequently, the operating parameters to be used as input to the created model were obtained from the experimental data in the literature. This allows for a comparison of our model's results with the experimental results under the same conditions.

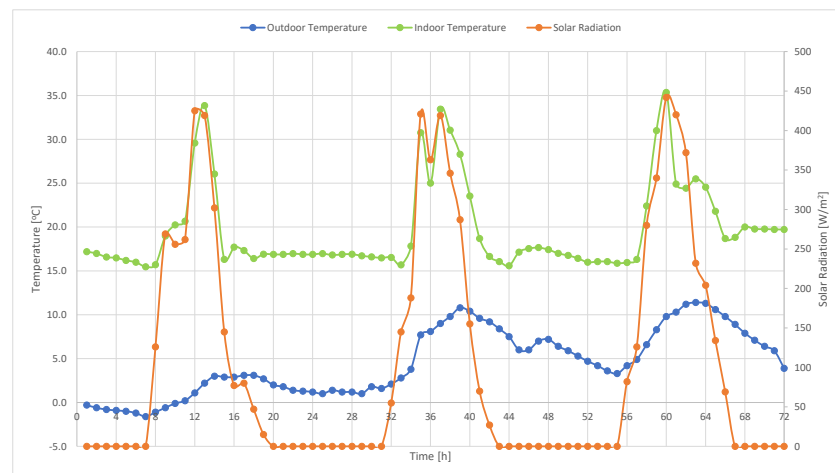


**Figure 3.** Digitized experimental data obtained from the study of Ahamed et al. [11].

For the transient system analysis, TRNSYS software, which is widely used in this field, was employed. TRNSYS is a comprehensive and extensible simulation environment for the transient simulation of systems, including multi-zone buildings [33]. While setting up the TRNSYS model, the 3D model of the greenhouse was first created in SketchUp 2021 software. The created greenhouse is shown in Figure 4.

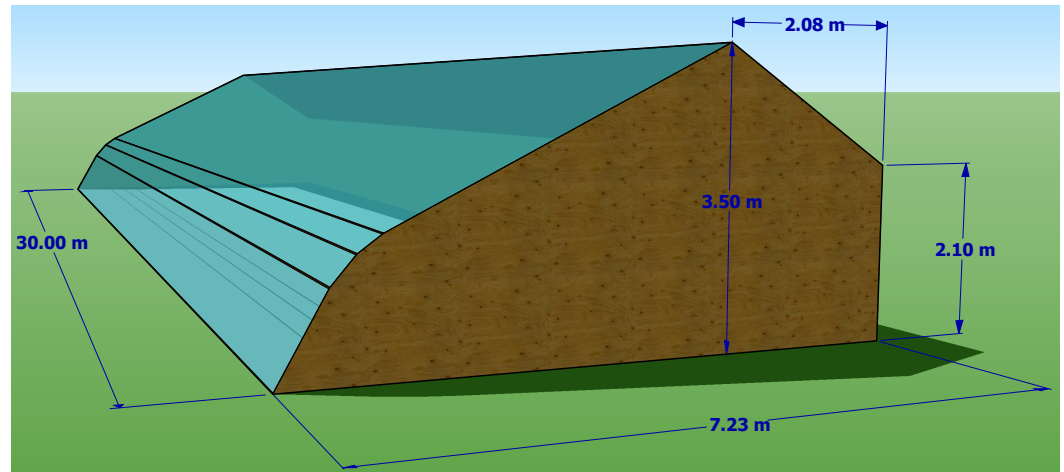


Figure 4. 3D CSG model created with SketchUp.

In TRNSYS, each operation is performed in modules (Types) and connections are established between them (Figure 5). The building materials and dimensions of the greenhouse are stored in Type 56—Multi-Zone Building. The location information to be examined is set in Type 15—Weather Data Processor by selecting from the TRNSYS library. Since evapotranspiration depends on outdoor temperature and solar energy, it varies widely throughout the day. Therefore, a separate module was created to calculate the evapotranspiration heat based on time. Results can also be obtained both visually and in tabular form using appropriate modules.

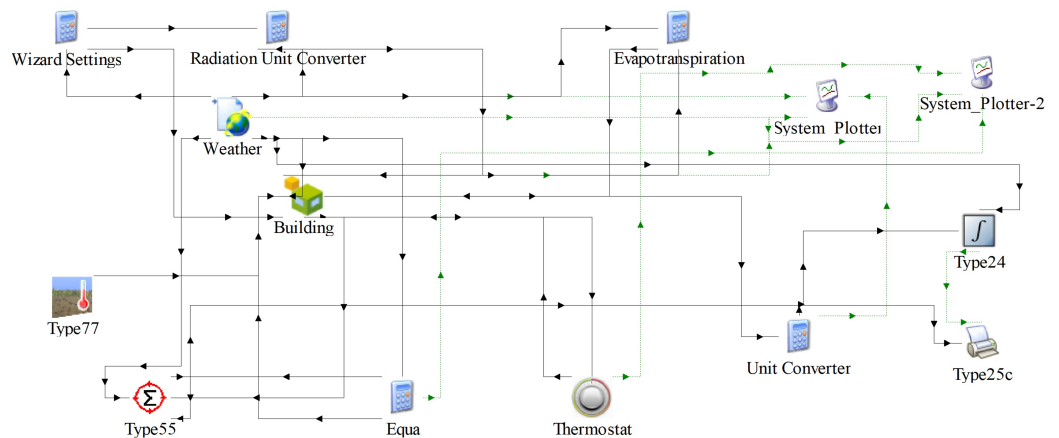
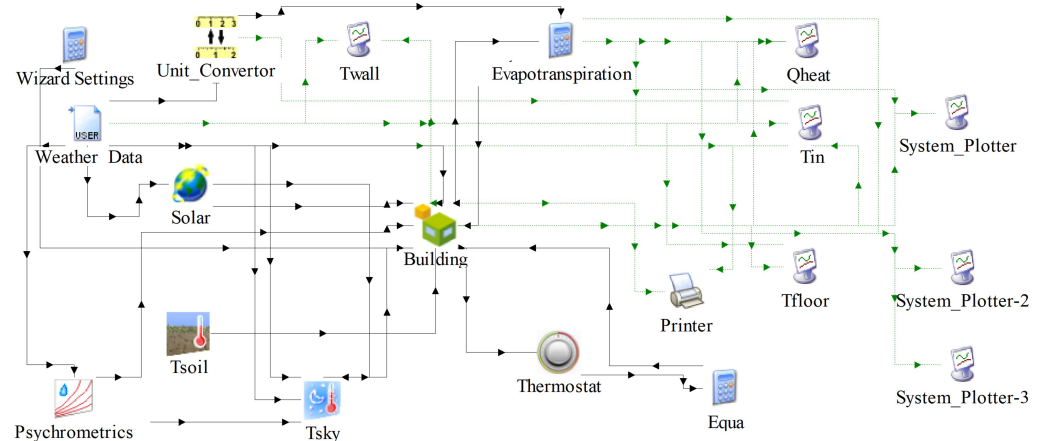


Figure 5. Created TRNSYS model.

### 2.3. Validation of TRNSYS Model

Type 15—Weather Data Processor is created by default, as location information is also entered when a 3D model drawn with SketchUp is transferred to TRNSYS. Since experimental measurements will be used as weather conditions in the validation part of our study, Type 15 was deleted and replaced with Type 9—Data Reader for Generic Data Files (Figure 6). This module allows the experimental measurement results to be used as inputs to the model. Solar radiation incident on the surfaces was calculated for all slopes and directions using the Type 16—Solar Radiation Processor, and connections were made to the relevant surfaces one by one. As a result, the model was ensured to operate under the same conditions as the experimental data.



**Figure 6.** TRNSYS model modified for the validation study.

The transparent surface used in the experimental study [11] is not included in the standard TRNSYS library. This surface must be correctly added to the model, as it is where solar energy is absorbed indoors. For this purpose, using Berkeley Lab Window v7.8.28.0, a surface was created according to the specifications given in the experimental study and added to the TRNSYS library.

To validate the created model, the indoor temperature and additional heating requirements given by Ahamed et al. [11] were discussed. They conducted their experiments for 3 days. The soil cable heating system, which was not operated on the first two nights, was operated on the third night. As this causes additional heat gain, it disrupts the compatibility with the model. For this reason, only the first two days' data were used for validation.

Statistical analysis was performed to evaluate the agreement with the experimental data. For this purpose, let  $n$ ,  $y_e$ ,  $y_m$ , and  $\bar{y}$  represent the number of data points, estimated data, measured data, and mean value of measured data, respectively. The coefficient of determination ( $R^2$ ), percent error ( $PE$ ), root mean square error ( $RMSE$ ) and relative root mean square error ( $rRMSE$ ) values were calculated as follows:

$$R^2 = 1 - \frac{\sum(y_m - y_e)^2}{\sum(y_m - \bar{y})^2} \quad (7)$$

$$PE = \frac{(y_m - y_e)}{y_m} \times 100 \quad (8)$$

$$RMSE = \sqrt{\frac{\sum(y_m - y_e)^2}{n}} \quad (9)$$

$$rRMSE = \frac{100}{\bar{y}} \times \sqrt{\frac{\sum(y_m - y_e)^2}{n}} \quad (10)$$

In Figure 7, the comparison of the indoor temperatures obtained from the simulation with the experimental measurements is given with 10% error bars. When the results are analyzed, it is seen that the maximum percent error and mean percent error are 20.3 and 0.4, respectively.  $R^2$ ,  $RMSE$  and  $rRMSE$  values are 0.95, 1.1 °C, and 5.9%, respectively. The results show that the model can accurately predict the indoor temperature with a low margin of error.

In Figure 8, experimental results and simulation results are compared in terms of additional heating requirements. 5% error bars were also added to the simulation results. The maximum percent error and average percent error are 4.9 and 0.1, respectively.  $R^2$ ,  $RMSE$  and  $rRMSE$  values are 0.99, 252 kJ/h, and 3.7%, respectively. The results show that the model can also predict the additional heating requirements with acceptable accuracy.

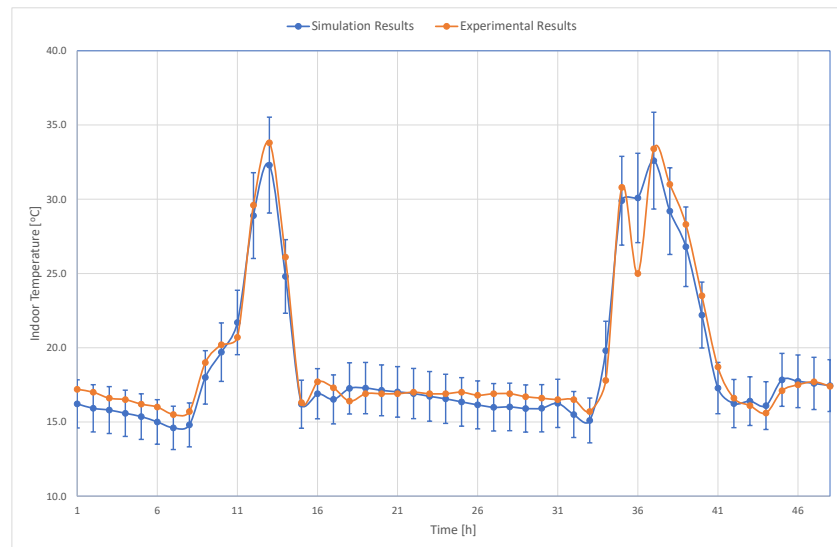


**Figure 7.** Comparison of the experimental and the simulation indoor temperatures.

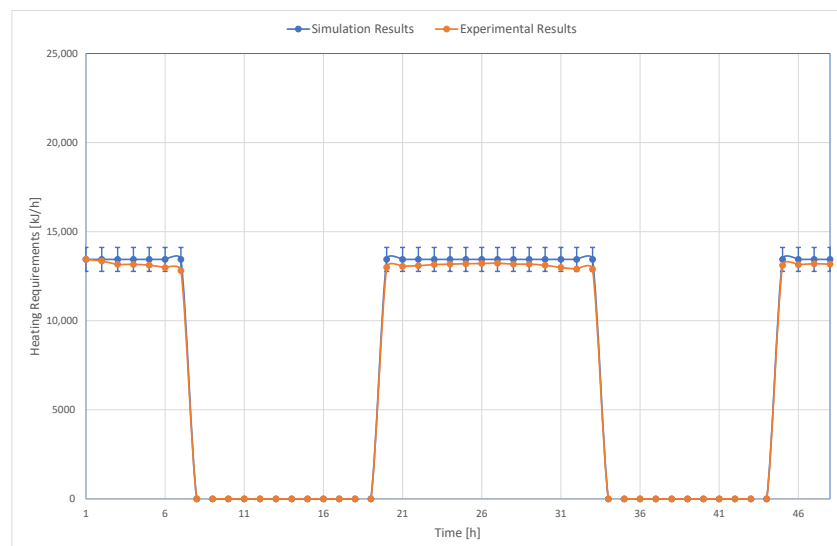


**Figure 8.** Comparison of experimental and simulation additional heating requirements.

When the results given in Figures 7 and 8 are examined, it is seen that our TRNSYS model can be used to determine the indoor temperatures and additional heating requirements of a CSG.

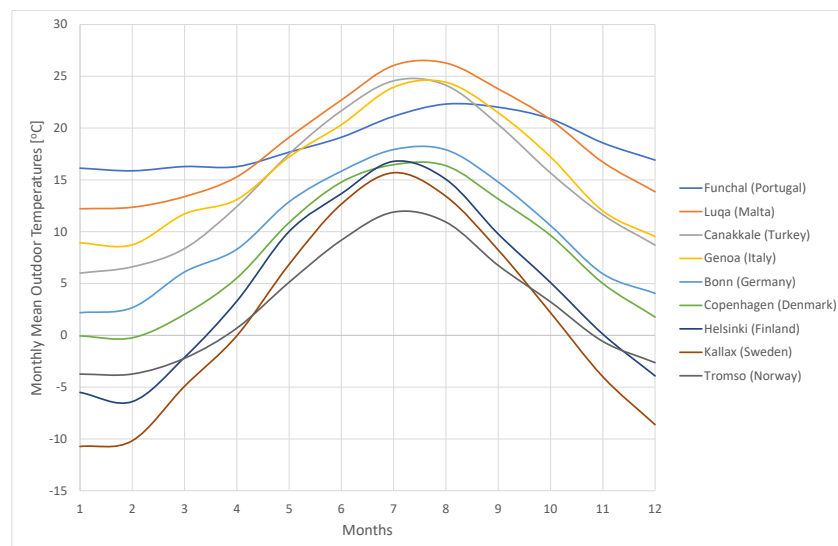
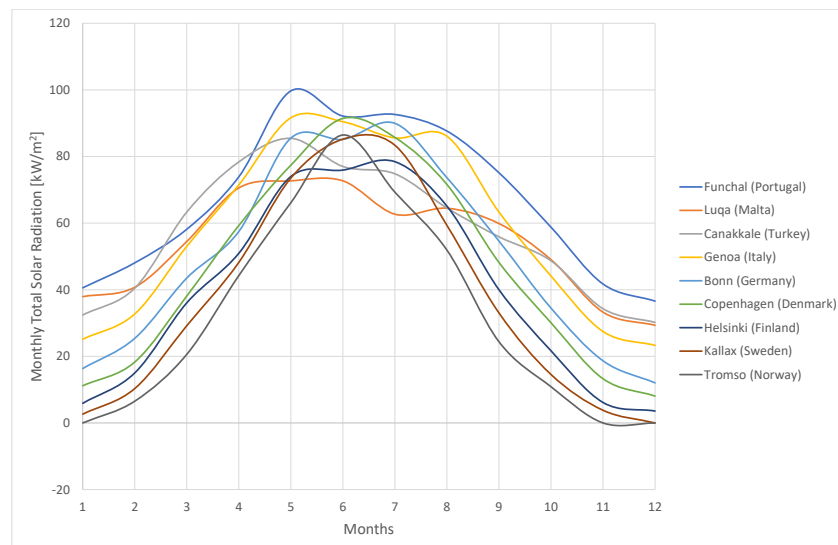
### 3. Results and Discussion

To investigate the performance of CSGs in different geographical locations, cities from the TRNSYS library, ranging approximately from the southernmost (Funchal, Portugal) to the northernmost (Tromsø, Norway) of Europe, were selected (Table 1). In selecting the cities, care was taken to ensure that the latitude difference between the cities averaged  $5^{\circ}$ . The purpose of varying the latitude is to modify the climate data. To minimize the impact of elevation on climate data, the selected provinces were chosen to be as close to sea level as possible. The aim here is to reveal the effect of latitude change on the performance of the CSG.

**Table 1.** Selected cities and location information from TRNSYS library.

No	Country	Location	Latitude [° N]	Longitude [° E]	Elevation [m]
1	Portugal (PT)	Funchal	32.63	−16.9	56
2	Malta (MT)	Luqa	35.83	14.43	135
3	Turkey (TR)	Canakkale	40.13	26.4	3
4	Italy (IT)	Genoa	44.42	8.85	3
5	Germany (DE)	Bonn	50.7	7.15	65
6	Denmark (DK)	Copenhagen	55.67	12.3	28
7	Finland (FI)	Helsinki	60.17	24.95	9
8	Sweden (SE)	Kallax	65.55	22.13	16
9	Norway (NO)	Tromso	69.65	18.95	102

The monthly mean outdoor temperatures and total solar radiation of the selected cities are given in Figure 9 and Figure 10, respectively. As expected, temperatures and solar radiation are high in the south. These values decrease towards the north. These values closely affect both the heat loss of the CSG to the environment and the heat gain from the sun.

**Figure 9.** Monthly mean outdoor temperatures of the selected cities for analysis.**Figure 10.** Monthly total solar radiation of the selected cities for analysis.

Consistent with the results of Beshada [10], the daytime indoor temperatures were more dependent on solar radiation than on outdoor temperatures. At night, since there is no solar radiation, the indoor temperature varies mainly depending on the outdoor temperature. The CSG monthly mean indoor temperature values are given in Figure 11 when no additional heater is used. The hourly indoor temperatures for all cities were found to be close to the outdoor temperature at night and well above the outdoor temperature during the daytime. For this reason, the daytime indoor temperatures of cities in the southern latitudes, which receive more solar energy, have also increased the mean value. Conversely, the mean indoor temperatures were found to be lower in cities at northern latitudes.

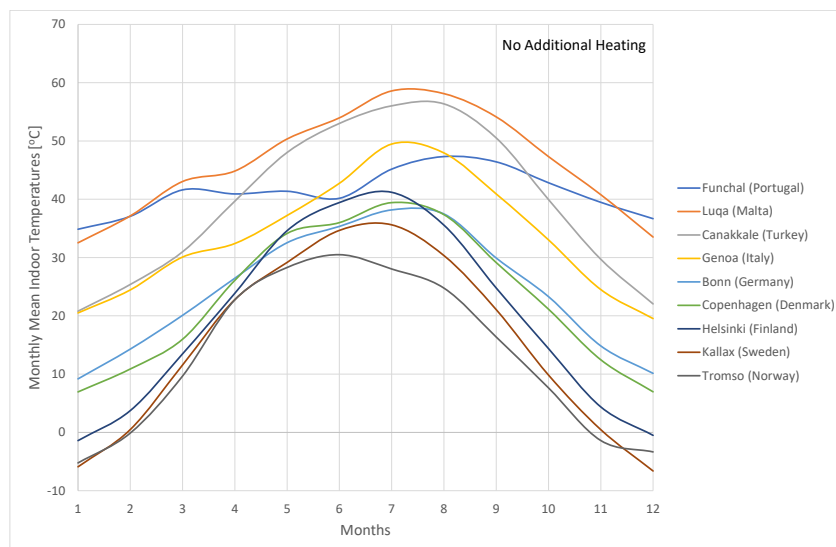


**Figure 11.** CSG monthly mean indoor temperatures without additional heater.

To be able to grow plants in the greenhouse in winter, it is not desirable for the CSG indoor temperature to fall below a certain value. For this purpose, an additional heater is used in the system. This additional heater is operated when the CSG indoor temperature falls below 16 °C and is turned off when it rises above 20 °C. The control of the additional heater is done with the thermostat in the model. Figure 12 shows the increase in the monthly mean indoor temperatures when the heater is used, compared to when the heater is not used. Since the minimum indoor temperatures were set to 16 °C with the additional heater, the minimum of the averages approached 16 °C, unlike in Figure 11. Since the outdoor temperature does not decrease much at night and the need for heating is already low in southern cities where the daytime sun is intense, the increase in the indoor temperature with heating was also low. In fact, in Funchal and Luqa, the two southernmost cities of our study, additional heating did not increase the monthly mean indoor temperature. Towards the north, due to the low outdoor temperature and low solar radiation, the heating effect has increased, and the indoor temperatures have increased.

When examined hourly, it is seen that the daytime indoor temperatures can reach 50 °C in winter, especially in southern cities. Since excess temperature is harmful to plants, the indoor temperature should be lowered in a controlled manner. At this point, it is possible to take advantage of the fact that the daytime indoor temperature is more dependent on solar radiation than on outdoor temperature. The outdoor air, which is at a lower temperature than the indoor temperature, can be taken in through the ventilation openings, allowing the environment to cool naturally and reach the desired temperature.

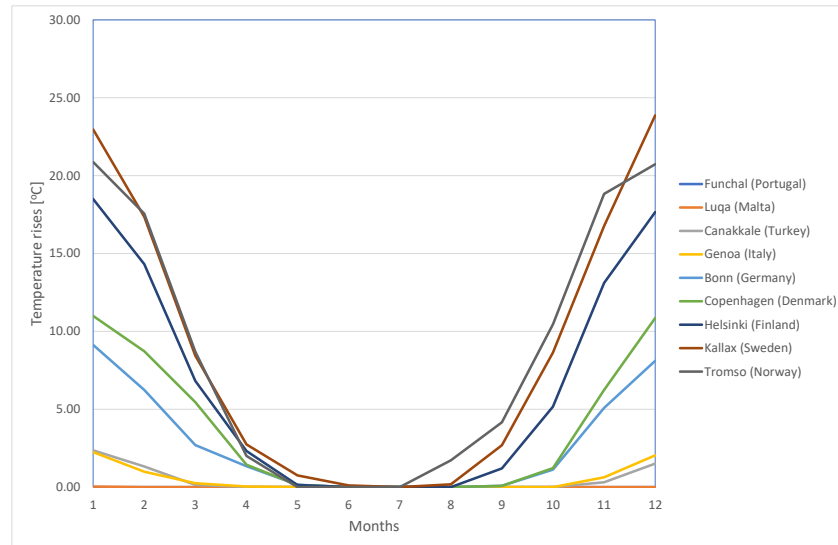


**Figure 12.** Increase in the monthly mean indoor temperatures of the CSG when the additional heater is used.

The annual total energy consumption of the additional heater used to provide the minimum set point temperature is given in Figure 13. Heating requirements in cities in cold northern latitudes are relatively high, while heating requirements decrease towards the south. For Funchal and Malta, seen in Figure 12, the heating requirements are also zero, as there is no year-round temperature increase with additional heating. Since the annual heating requirement in Malta is as low as  $0.15 \text{ kW/m}^2$ , it is accepted as zero. As the latitude increases, that is, towards the north, the heating requirements in general also increase. Also in Figure 13, the duration of the heating season is indicated in months. It has been demonstrated that year-round heating is required in Tromso, the northernmost city.

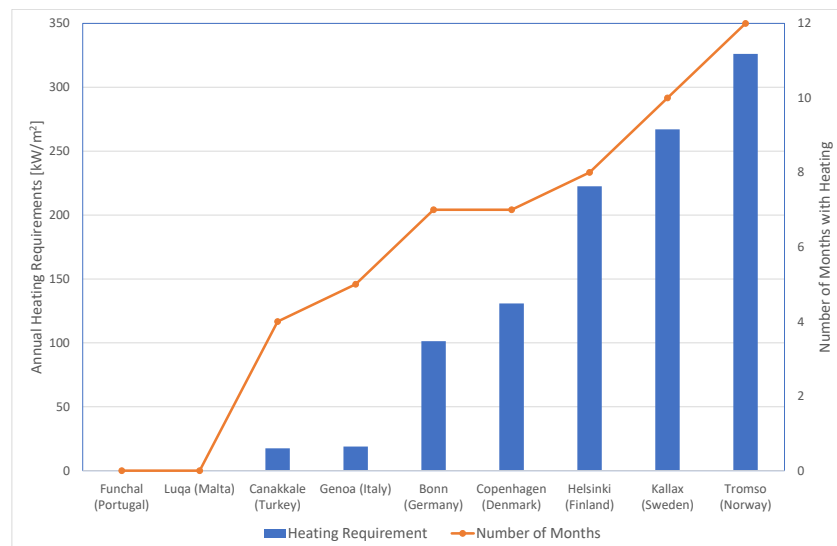


**Figure 13.** CSG's annual heating requirements and durations.

At night, when solar energy cannot be utilized, the transparent south roof of the CSG is covered with a thermal covering. Thus, night heat loss is minimized. In practice, the thermal covering is easy to operate on a fixed schedule. However, this is quite inefficient as it is done without considering solar energy momentarily. Instead, it is necessary to control based on solar energy. In our study, the thermal covering was kept open during the hours when solar energy could not be used. This has been done through a module added to the TRNSYS model. Depending on the cities, the open times of the thermal covering are given

in Figure 14. This value is higher in cities in northern latitudes, where the sun exposure time is less in winter. In summer, as the sunshine duration is longer and nights are shorter in high northern latitudes, the open time of the covering is relatively shorter.

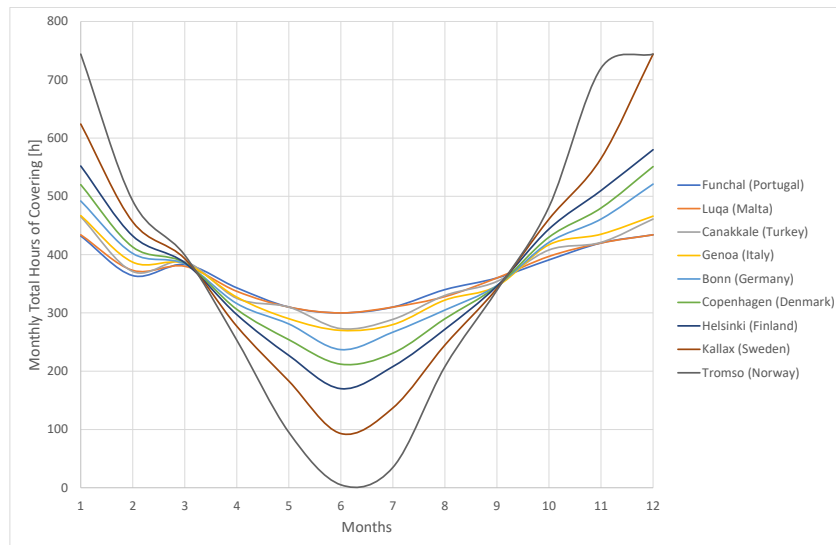


Figure 14. Open times of the thermal covering.

The thermal covering used significantly reduces the heating requirements. This decrease is shown in Figure 15. If the cities of Funchal, Portugal (32.63° N) and Luqa, Malta (35.83° N), where the requirement for additional heating is zero when the thermal covering is used, are excluded from the analysis, it can be seen from Figure 15 that the benefit ratio (BR) of the thermal covering (Equation (11)) changes between the cities in the south and the north. This is related to the outdoor temperature at night when the thermal covering is used. The thermal covering of the same material and thickness loses less heat at the higher nighttime outdoor temperatures. As the outdoor temperature decreases, the heat loss increases. Therefore, the use of thermal coverings in cities located in the relatively south, such as Canakkale, Turkey (40.13° N) and Genoa, Italy (44.42° N) further reduces the requirement for additional heating. Conversely, covering reduces the heating requirement less in the northern cities of Kallax, Sweden (65.55° N) and Tromso, Norway (69.65° N).

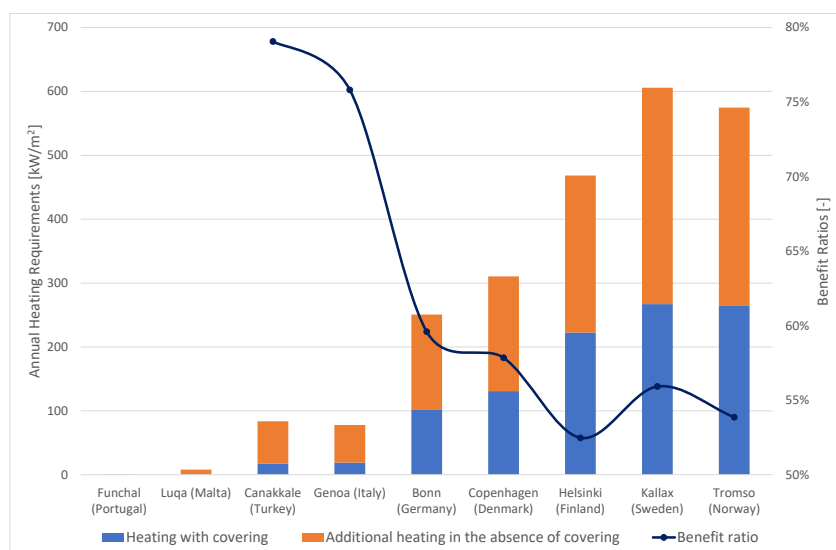
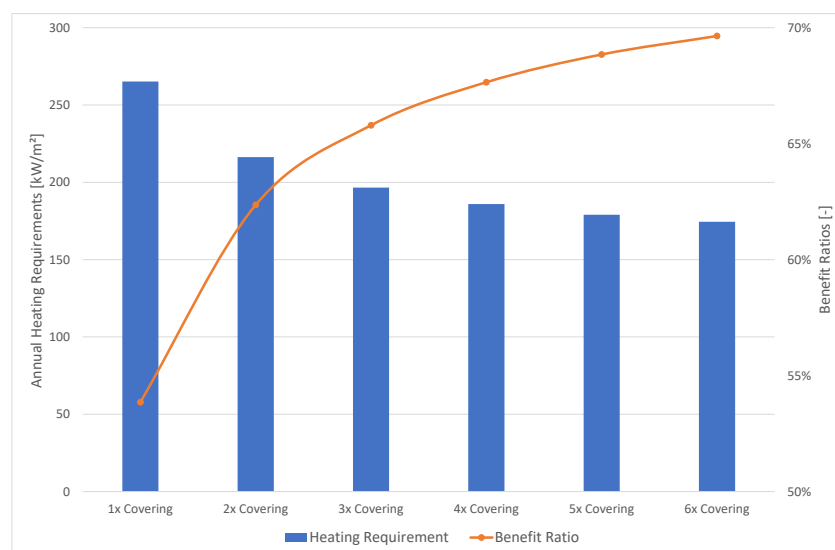


Figure 15. Annual heating requirements and benefit ratios based on thermal covering usage.

$$BR = 1 - \frac{\text{Heating requirement with covering}}{\text{Heating requirement without covering}} \quad (11)$$

To increase the BR of Tromso, the northernmost city, an investigation was made by increasing the thickness of the covering material. As can be seen in Figure 16, it was found that BR could be increased up to 70% in this city. Although increasing the thickness of the thermal covering reduces the heating requirement, in Tromso, it has been found that the heating requirement remains throughout the year.



**Figure 16.** Annual Heating Requirements and benefit ratios of the CSG in Tromso (Norway).

#### 4. Conclusions

TRNSYS, which has a large weather database, is frequently used in the analysis of solar energy systems. In this study, a CSG model was created using TRNSYS and validated with experimental data. Then, the use of CSG for cities in different latitudes of Europe was investigated. The study was carried out throughout the year, focusing on the heating needs necessary for winter. The results of this study reveal the suitability of using CSG in plant breeding for Europe in general. The study also highlights possible improvements and developments. The main results of the study are as follows:

- In the study, nine different cities in Europe were selected based on their latitudes to alter their climate data. These cities are between 32.63° N and 69.65° N latitude and are spread approximately from the southernmost to the northernmost in Europe. Thus, results were obtained across a very wide latitude range.
- The CSG indoor temperatures and corresponding heating requirements were found to depend on solar energy during the daytime and the outdoor temperature during nighttime.
- In temperate southern cities with intense sun, the need for heating in winter is low. In Funchal, Portugal (32.63° N) and Luqa, Malta (35.83° N), heating was not even required in winter.
- Towards the north, the requirement for heating increased. Despite the prolongation of sunshine duration, the decrease in solar radiation and outdoor temperature caused this increase. It has also been shown that the heating requirement in Tromso exists for 12 months of the year.
- The use of thermal covering significantly reduces the need for heating. Since control according to a fixed schedule leads to inefficiency, transient control based on solar energy was implemented. The use of thermal covering of the same material and thickness reduced the heating requirement by 50–80% depending on the location. It

has been shown that in cold northern regions where this decrease is low, the benefit ratio of the covering can be increased up to 70% by increasing the covering thickness.

- Since the cities were selected to be approximately at sea level to eliminate the effects of elevation, the results obtained based solely on latitude cannot be generalized. Different results may be obtained at the same latitude but in a high mountainous region, depending on temperature and solar radiation. Future studies could consider the variations in temperature and solar radiation due to elevation.

**Author Contributions:** Conceptualization, S.E. and C.O.; methodology, S.E. and C.O.; software, S.E.; validation, S.E.; formal analysis, S.E. and C.O.; investigation, C.O.; resources, S.E.; data curation, S.E.; writing—original draft preparation, S.E. and C.O.; writing—review and editing, S.E. and C.O.; visualization, S.E. and C.O.; supervision, S.E. and C.O.; project administration, S.E.; funding acquisition, S.E. and C.O. All authors have read and agreed to the published version of the manuscript.

**Funding:** This research received no external funding.

**Data Availability Statement:** The data presented in this study are available on request from the corresponding author.

**Conflicts of Interest:** The authors declare no conflicts of interest.

## Abbreviations

The following abbreviations are used in this manuscript:

$A_p$	area of plant [m <sup>2</sup> ]
$I_g$	global solar radiation on horizontal surface [W/m <sup>2</sup> ]
$L_f$	characteristic length of plant leaves [m]
$L_v$	latent heat of water vaporization [J/kg]
$M_T$	moisture transfer rate [kg/s]
$n$	number of data points
$P$	atmospheric pressure [kPa]
$P_w$	partial pressure of the water vapor [kPa]
$P_{ws}$	partial pressure at saturation [kPa]
$Q_e$	evapotranspiration heat transfer rate [W]
$R_a$	aerodynamic resistance [s/m]
$R_s$	stomatal resistance [s/m]
$v_i$	indoor airspeed [m/s]
$w_i$	humidity ratio of air at indoor temperature [kg/kg]
$w_{ps}$	saturated humidity ratio of air at plant temperature [kg/kg]
$y_e$	estimated data
$y_m$	measured data
$\bar{y}$	mean value of measured data
$\rho_{air}$	density of air [kg/m <sup>3</sup> ]
$\tau$	transmissivity of cover

## References

1. Tong, G.; Christopher, D.M.; Li, T.; Wang, T. Passive solar energy utilization: A review of cross-section building parameter selection for Chinese solar greenhouses. *Renew. Sustain. Energy Rev.* **2013**, *26*, 540–548. [[CrossRef](#)]
2. Chen, W.; Liu, W. Numerical simulation of the airflow and temperature distribution in a lean-to greenhouse. *Renew. Energy* **2006**, *31*, 517–535. [[CrossRef](#)]
3. Meng, L.; Yang, Q.; Bot, G.P.A.; Wang, N. Visual simulation model for thermal environment in Chinese solar greenhouse. *Trans. Chin. Soc. Agric. Eng.* **2009**, *25*, 164–170.
4. Singh, G.; Singh, P.P.; Lubana, P.P.S.; Singh, K.G. Formulation and validation of a mathematical model of the microclimate of a greenhouse. *Renew. Energy* **2006**, *31*, 1541–1560. [[CrossRef](#)]
5. Ma, C.W.; Han, J.J.; Li, R. Research and development of software for thermal environmental simulation and prediction in solar greenhouse. *North. Hortic.* **2010**, *15*, 69–75.
6. Tong, G.; Christopher, D.M.; Li, B. Numerical modelling of temperature variations in a Chinese solar greenhouse. *Comput. Electron. Agric.* **2009**, *68*, 129–139. [[CrossRef](#)]

7. Wang, X.W.; Luo, J.Y.; Li, X.P. CFD Based Study of Heterogeneous Microclimate in a Typical Chinese Greenhouse in Central China. *J. Integr. Agric.* **2013**, *12*, 914–923. [[CrossRef](#)]
8. Zhang, G.; Fu, Z.; Yang, M.; Liu, X.; Dong, Y.; Li, X. Nonlinear simulation for coupling modeling of air humidity and vent opening in Chinese solar greenhouse based on CFD. *Comput. Electron. Agric.* **2019**, *162*, 337–347. [[CrossRef](#)]
9. Vivekanandan, M.; Periasamy, K.; Babu, C.D.; Selvakumar, G.; Arivazhagan, R. Experimental and CFD investigation of six shapes of solar greenhouse dryer in no load conditions to identify the ideal shape of dryer. *Mater. Today Proc.* **2020**, *37*, 1409–1416. [[CrossRef](#)]
10. Beshada, E.; Zhang, Q.; Boris, R. Winter performance of a solar energy greenhouse in southern Manitoba. *Can. Biosyst. Eng./Le Genie des Biosyst. au Canada* **2006**, *48*, 1–8.
11. Ahamed, M.S.; Guo, H.; Tanino, K. Development of a thermal model for simulation of supplemental heating requirements in Chinese-style solar greenhouses. *Comput. Electron. Agric.* **2018**, *150*, 235–244. [[CrossRef](#)]
12. Ahamed, M.S.; Guo, H.; Tanino, K. Modeling heating demands in a Chinese-style solar greenhouse using the transient building energy simulation model TRNSYS. *J. Build. Eng.* **2020**, *29*, 101114. [[CrossRef](#)]
13. Dong, S.; Ahamed, M.S.; Ma, C.; Guo, H. A time-dependent model for predicting thermal environment of mono-slope solar greenhouses in cold regions. *Energies* **2021**, *14*, 5956. [[CrossRef](#)]
14. Liu, R.; Li, M.; Guzmán, J.L.; Rodriguez, F. A fast and practical one-dimensional transient model for greenhouse temperature and humidity. *Comput. Electron. Agric.* **2021**, *186*, 106186. [[CrossRef](#)]
15. Wei, B.; Guo, S.; Wang, J.; Li, J.; Wang, J.; Zhang, J.; Qian, C.; Sun, J. Thermal performance of single span greenhouses with removable back walls. *Biosyst. Eng.* **2016**, *141*, 48–57. [[CrossRef](#)]
16. Mobtaker, H.G.; Ajabshirchi, Y.; Ranjbar, S.F.; Matloobi, M. Simulation of thermal performance of solar greenhouse in north-west of Iran: An experimental validation. *Renew. Energy* **2019**, *135*, 88–97. [[CrossRef](#)]
17. Chen, J.; Ma, Y.; Pang, Z. A mathematical model of global solar radiation to select the optimal shape and orientation of the greenhouses in southern China. *Sol. Energy* **2020**, *205*, 380–389. [[CrossRef](#)]
18. Zhang, Y.; Henke, M.; Li, Y.; Xu, D.; Liu, A.; Liu, X.; Li, T. Towards the maximization of energy performance of an energy-saving Chinese solar greenhouse: A systematic analysis of common greenhouse shapes. *Sol. Energy* **2022**, *236*, 320–334. [[CrossRef](#)]
19. Liu, X.; Wu, X.; Xia, T.; Fan, Z.; Shi, W.; Li, Y.; Li, T. New insights of designing thermal insulation and heat storage of Chinese solar greenhouse in high latitudes and cold regions. *Energy* **2022**, *242*, 122953. [[CrossRef](#)]
20. Wang, J.; Li, S.; Guo, S.; Ma, C.; Wang, J.; Jin, S. Simulation and optimization of solar greenhouses in Northern Jiangsu Province of China. *Energy Build.* **2014**, *78*, 143–152. [[CrossRef](#)]
21. Yu, Y.; Xu, X.; Hao, W. Study on the wall optimization of solar greenhouse based on temperature field experiment and CFD simulation. *Int. J. Heat Technol.* **2018**, *36*, 847–854. [[CrossRef](#)]
22. Sethi, V.P. On the selection of shape and orientation of a greenhouse: Thermal modeling and experimental validation. *Sol. Energy* **2009**, *83*, 21–38. [[CrossRef](#)]
23. Gupta, R.; Tiwari, G.N.; Kumar, A.; Gupta, Y. Calculation of total solar fraction for different orientation of greenhouse using 3D-shadow analysis in Auto-CAD. *Energy Build.* **2012**, *47*, 27–34. [[CrossRef](#)]
24. El-Maghlany, W.M.; Teamah, M.A.; Tanaka, H. Optimum design and orientation of the greenhouses for maximum capture of solar energy in North Tropical Region. *Energy Convers. Manag.* **2015**, *105*, 1096–1104. [[CrossRef](#)]
25. Çakir, U.; Şahin, E. Using solar greenhouses in cold climates and evaluating optimum type according to sizing, position and location: A case study. *Comput. Electron. Agric.* **2015**, *117*, 245–257. [[CrossRef](#)]
26. Stanciu, C.; Stanciu, D.; Dobrovicescu, A. Effect of Greenhouse Orientation with Respect to E-W Axis on its Required Heating and Cooling Loads. *Energy Procedia* **2016**, *85*, 498–504. [[CrossRef](#)]
27. Chen, C.; Li, Y.; Li, N.; Wei, S.; Yang, F.; Ling, H.; Yu, N.; Han, F. A computational model to determine the optimal orientation for solar greenhouses located at different latitudes in China. *Sol. Energy* **2018**, *165*, 19–26. [[CrossRef](#)]
28. Ahamed, M.S.; Guo, H.; Tanino, K. A quasi-steady state model for predicting the heating requirements of conventional greenhouses in cold regions. *Inf. Process. Agric.* **2018**, *5*, 33–46. [[CrossRef](#)]
29. Nobel, P.S. *Introduction to Biophysical Plant Physiology*; Series of Books in Biology; W. H. Freeman and Company: San Francisco, CA, USA, 1974.
30. Albright, L. *Environment Control for Animals and Plants*; ASAE Textbook [Series]; American Society of Agricultural Engineers: St. Joseph, MI, USA, 1990.
31. Boulard, T.; Wang, S. Greenhouse crop transpiration simulation from external climate conditions. *Agric. For. Meteorol.* **2000**, *100*, 25–34. [[CrossRef](#)]
32. Boulard, T.; Baille, A.; Le Gall, F. Study of various cooling methods and their effect on microclimate and transpiration of a greenhouse tomato crop [climatisation, static ventilation]. *Agronomie (France)* **1991**, *11*, 543–553.
33. Klein, S.A. *TRNSYS 18: A Transient System Simulation Program*; University of Wisconsin-Madison: WI, USA, 2018.

**Disclaimer/Publisher’s Note:** The statements, opinions and data contained in all publications are solely those of the individual author(s) and contributor(s) and not of MDPI and/or the editor(s). MDPI and/or the editor(s) disclaim responsibility for any injury to people or property resulting from any ideas, methods, instructions or products referred to in the content.